HHS Public Access

Author manuscript

J Comput Assist Tomogr. Author manuscript; available in PMC 2018 May 01.

Published in final edited form as:

J Comput Assist Tomogr. 2017 ; 41(3): 505–510. doi:10.1097/RCT.0000000000000557.

The effect of patient diameter on the dual-energy ratio of selected contrast-producing elements

Jack W. Lambert, PhD[1], **Paul F. FitzGerald, AAS**[2], **Peter M. Edic, PhD**[2], **Yuxin Sun, MS**[1], **Peter J. Bonitatibus Jr, PhD**[2], **Robert E. Colborn, PhD**[2], and **Benjamin M. Yeh, MD**[1]

[1]Department of Radiology and Biomedical Imaging, University of California, San Francisco, 505 Parnassus Ave, San Francisco, CA 94143

[2]GE Global Research, 1 Research Circle, Niskayuna, NY 12309

Abstract

Objectives—To assess whether the low- to high-kVp CT number ratio at dual-energy CT (DECT) is affected by changes in patient diameter.

Methods—Seven contrast-producing elements were housed sequentially within an abdomen phantom. Fat rings enlarged the phantom diameter from 26 to 45 cm. The phantom was scanned using single-energy CT (SECT) at tube potentials of 80 and 140 kVp, and rapid-kVp-switching DECT.

Results—CT numbers decreased proportionally (~20% CT number reduction for smallest to largest phantom diameters) for low- and high-energy acquisitions, but resulted in consistent dual-energy ratios for each contrast element. For 17/21 material pair combinations, the dual-energy ratio ranges of the two elements did not overlap, implying that discrimination should remain possible for these material pairs at all patient sizes.

Conclusions—The dual-energy ratio for different contrast materials is largely unaffected by changes in phantom diameter. This should allow for robust separation of most contrast material combinations irrespective of patient size.

Keywords

dual-energy CT; contrast media; high-Z elements; dual-energy ratio

Introduction

Dual-energy CT (DECT) has emerged as a valuable diagnostic tool and offers additional material-specific information compared to single-energy CT (SECT).(1) This material discrimination is made possible by exploiting the different attenuation properties of different materials when imaged using low- versus high-energy x-ray spectra. A given element's attenuation profile depends on both the atomic number and the physical density of the material, due to the photoelectric absorption effect and Compton scattering, the two

Corresponding author: Jack W Lambert, Department of Radiology and Biomedical Imaging, University of California, San Francisco, 505 Parnassus Ave, San Francisco, CA 94143, Tel: 415-514-0507, Fax: 415-476-0616, jack.lambert@ucsf.edu.

dominant attenuation mechanisms at diagnostic energy levels.(2) As DECT operates with low-energy (usually 80 kVp) and high-energy (usually 140 kVp) x-ray spectra, the relative attenuation of voxels in the imaged volume at these two spectra (or, commonly referred as "energies", although the applied spectra contain a continuous distribution of energies) is acquired.

The relative difference in attenuation at the two energies forms the basis for material decomposition. The greater the difference in attenuation profile between two materials, the easier the decomposition of the materials' signal at DECT.(2–6) Screening different materials for their separability at DECT is commonly achieved by reference to the low- to high-kVp CT number ratio for each material, a metric known as the dual-energy ratio (DER). Falt *et al.*(7) showed that candidate high-Z contrast elements offer low DERs (DER ~ 1–1.5) that are distinct from existing clinical iodine and barium-based agents (DER ~ 2), and are thus attractive for dual-contrast DECT studies. Gabbai *et al.*(8) demonstrated that these DERs remain consistent between different DECT platforms. Other studies have screened high-Z contrast elements for their imaging efficacy at different x-ray spectra, but have not investigated dual-energy properties.(9, 10)

An important but largely unexplored aspect of a given material's DER is its potential dependency on patient size, due to its attenuation characteristics and the beam-hardening effect. Beam hardening is a phenomenon whereby low-energy x-ray photons are preferentially absorbed, increasing the mean photon energy of the detected x-ray spectrum and therefore lowering measured CT numbers in the reconstructed images.(11) This effect is more pronounced in larger patient sizes because x-rays are attenuated over longer material path lengths.(12) Beam hardening may adversely affect the robustness of using the DER as a means for material separation, particularly between elements of relatively similar DER where discrimination is already challenging, such as iodine and calcium. Recent research has provided encouraging results; Krauss *et al.*(13) imaged iodinated contrast material in circular phantoms 10–40 cm in diameter using dual-source CT (DSCT). Although the primary aim of the study was to investigate different energy and filtration options, the DER for iodine remained unchanged by phantom size. Other elements potentially useful for CT contrast were not tested.

The aim of our study is to further characterize how the DER of different elements is influenced by patient size. We sought to achieve this through thorough investigation of seven different elements which are currently used or have been proposed for use as future CT contrast agents, over a range of phantom sizes representing small to obese adults.

Materials and Methods

Phantoms

A pseudo-anthropomorphic adult abdomen phantom (Model 007TE, CIRS, Norfolk, VA) composed of soft-tissue-equivalent plastic, measuring 220 mm in the anterior-posterior (AP) diameter, 300 mm in the lateral (LAT) diameter, and 150 mm in length, was used for all scanning (Figure 1 a). A 150-mm long, 19-mm outside diameter, cylindrical vial made of poly (methyl methacrylate) (PMMA) was filled with the contrast material to be tested and

was centrally located in the phantom. The phantom was encased sequentially in three differently-sized clamshell-type rings composed of adipose-equivalent plastic, measuring 33, 60, and 90 mm in thickness (Fig 1 b–d) (Table 1). The rings simulated effective patient diameters, defined as $\sqrt{AP \times LAT}$, (14) from 257 to 438 mm for the thinnest (0 mm for base phantom) to thickest fat ring configuration (Table 1).

Contrast elements

Seven contrast elements with a wide range of atomic numbers were formulated according to Table 2. We chose elements including three currently-used clinical contrast agents: iodine, barium, and gadolinium.(15) Three high-Z elements that are candidates for future clinical CT contrast agents - tantalum, tungsten, and bismuth - were also included.(9, 16–19) Calcium was tested because it represents a common biological material to be separated from contrast agents at DECT.(4) Each element except calcium was formulated in distilled water at a concentration of 10 mg active element/mL, which approximates concentrations representative of those observed clinically.(8–10, 20) Calcium was suspended at a concentration of 30 mg/mL to represent arterial calcium deposits and bone.(8) Control vials with water in place of a contrast element were also scanned at each phantom size.

CT scanning

All imaging used a clinical rapid-kVp-switching DECT (rsDECT) scanner (Discovery CT750HD, GE Healthcare, Little Chalfont, UK). Scans were performed in axial mode with a collimation of 40 mm (64 × 0.625-mm detector rows), a large-patient bow-tie filter, and without use of automatic exposure control. Three scans were performed: SECT scans at 80 and 140 kVp, and a rsDECT scan at the same x-ray tube operating voltages. Tube currents and DECT Gemstone Spectral Imaging (GSI, GE Healthcare) protocol presets were adapted according to the phantom diameter (Table 1), in order to produce a similar level of image noise for each phantom configuration (Fig 1). These presets were chosen using a Noise Index (GE's image quality reference parameter) of 31, specified for a reconstructed image thickness of 2.5 mm.

Image analysis

All images were reconstructed with a thickness of 2.5 mm using filtered back-projection and the standard filtering kernel. For the DECT scans, images were reconstructed at Virtual Monochromatic Spectral (VMS) levels of 60 and 80 keV, to approximate the mean energy of the 80-kVp and 140-kVp SECT images.(8) Mean CT number measurements were taken from circular 1-cm^2 (5.6-mm radius) regions of interest (ROIs) placed in the center of the element-containing vial in 10 consecutive axial images. Bright streak artifacts from the spine insert affected the measurement region in the vial, particularly at 80 kVp for the large phantom sizes. We corrected for this by subtracting the CT number within a water vial, scanned under the same phantom configuration, from the CT number of each of the contrast vial. Although this did not eliminate the artifact itself, it adjusted the contrast vial CT numbers to levels unbiased by the artifactual brightness from the spine insert. We calculated DERs by dividing the CT number at 60 keV by the CT number at 80 keV for the VMS images, and by dividing 80-kVp CT numbers by 140-kVp CT numbers in the SECT images.

The DERs for the seven elements were compared to one another for a total of 21 material pairs. To assess whether discrimination of a material pair remained achievable at all phantom sizes, the range in the DER over the different phantom sizes were compared for each element. If the DER ranges of two elements did not overlap in either the VMS or the SECT images, the pair was considered separable.

Results

All elements showed a decreasing trend in CT number with increasing phantom diameter for the four image sets (60- and 80-keV DECT VMS, and 80- and 140-kVp SECT) (Fig 2). CT numbers decreased monotonically, with the exception of some of the elements in the 60-keV VMS images, in which gadolinium, tantalum, tungsten and, to a lesser extent, bismuth displayed sub-regions over which the CT numbers were nearly constant or even increased. Overall, the 60- and 80-keV VMS images generated via DECT provided similar CT numbers to the 80- and 140-kVp SECT images respectively, with a mean intra-element difference (difference between each VMS data point and the corresponding SECT data point) of 10.6 HU and a maximum difference of 43 HU for tungsten, due its non-linear behavior at 60-keV VMS (Fig 2 a). As the phantom size increased from 257 to 438 mm, the mean CT number of the elements across all image types decreased by ~20% (Fig 3). The decreases in CT number ranged from a minimum of 11% for bismuth at 140 kVp to a maximum of 31% for barium at 140 kVp. Overall, the high-Z elements tantalum, tungsten, and bismuth maintained a more constant attenuation over the range of phantom sizes than the conventional CT agents iodine, barium and gadolinium, with a mean CT number reduction of 14% for the high-Z elements compared to 26% for the conventional elements ($p<0.05$).

Dual-energy ratios

The DERs for 60:80-keV VMS (Fig 4 a) and 80:140-kVp SECT (Fig 4 b) remained consistent over the range of phantom sizes. This was due to the proportional decrease in CT number with increasing phantom size for both low- and high-energy spectra (Figs 2 and 3). The largest difference was observed for bismuth, with a variation between phantom sizes of 15.8% in the 80:140-kVp images. Iodine was the most consistent element, with a variation of 6.5% in the 60:80-keV VMS images and 1.4% in the 80:140-kVp SECT images. The DER ranges of the seven elements did not overlap in seventeen of the twenty-one pairs of elements, suggesting that material discrimination should remain possible for these pairs at all patient sizes (Table 3). The exceptions were iodine-barium, tungsten-tantalum, tungsten-bismuth, and tantalum-bismuth. Overall, the 60:80 keV VMS DERs agreed well with the 80:140 kVp DERs (Table 4). The largest difference was observed for tungsten at the 323 mm diameter phantom size, with a discrepancy between VMS and SECT DERs of 16.6%.

Discussion

Our study showed that dual-energy CT number ratios of clinical and proposed contrast elements do not change substantially with phantom size, despite reduction of CT numbers with increased object size. This is because the CT number reduction was approximately proportional at low and high x-ray energies, and thus the ratio between the two remained

similar. Our results suggest that dual-energy material discrimination algorithms using DER need not compensate for patient body habitus. Previous studies have reported decreasing CT numbers at larger simulated patient sizes due to beam hardening, but without phantoms as large as those used here or assessment of dual-energy properties.(9, 10) The DERs that were determined in our study agree well with those reported in literature, as obtained using a dual-source scanner, with the exception of bismuth.(7) In a previous study, the DER of bismuth was reported as 1.4, compared to ~1.0 in our experiments. This discrepancy may be a result of the previous study's choice of bismuth formulation. The authors used bismuth chloride ($BiCl_3$) as the solute, with hydrochloric acid (HCl) as the solvent, with a resulting high (>3:1) ratio of chlorine to bismuth atoms. As chlorine (Z=17) has a relatively high atomic number compared to organic compounds, its correspondingly high attenuation may have significantly altered the dual-energy ratio of the solution. With a similar atomic number to calcium (Z=20), chlorine has a positive dual-energy ratio, which would explain the reported ratio of 1.4. Our study used bismuth citrate ($C_6H_5BiO_7$) in a water-based suspension with xanthan gum ($C_{35}H_{49}O_{29}$), and as such the highest atomic number element other than bismuth was oxygen (Z=8). As such we believe the DER of ~1 reported here to be more representative of elemental bismuth.

Our second major finding is the smaller CT number decrease with increasing phantom size for the high-Z elements (tungsten, tantalum and bismuth) compared to the conventional elements (iodine, barium and gadolinium). Our measured results, which are determined using large physical phantoms, corroborate results of prior studies which used physical phantoms to image hafnium and tungsten,(18) and indirectly simulated large patient diameter with either computer simulations,(9) or through filtration of the x-ray source.(10) Our results highlight the advantage of potential non-iodinated high-Z agents for use in large-to-obese patients, given that 1) their low dual-energy ratios imply sustained contrast at the high-kVp settings required for this population, and 2) contrast enhancement by high-Z elements is not diminished by large patient size, unlike that of iodine and barium agents. Despite these imaging benefits, no high-Z contrast element is currently approved for clinical use, and as such, biocompatibility and toxicity remain uncertain.(10, 21) Gold and tungsten nanoparticle-based agents appear to show effective clearance, although data is limited to imaging studies tracking renal contrast enhancement.(19, 22) However, recent data for tantalum nanoparticle-based agents includes more detailed tolerability and clearance properties that appear promising for clinical translation.(23)

Our third major finding is the consistency in the CT numbers and DERs generated through SECT imaging compared to those generated with VMS images at DECT. All elements showed a decreasing trend of CT number versus phantom diameter which was well-matched between SECT and VMS images, with the exception of gadolinium tantalum, and tungsten which exhibited a flatter sub-region at 60 keV VMS. One concern with the nature of the VMS images is that these images are synthesized from a two-material decomposition using iodine and water (24), *i.e.* the basis materials, and don't account for the k-edges of gadolinium, tantalum, and tungsten. Those elements' k-edge energies (50, 67, and 70 keV, respectively) are near the approximately 60-keV mean energy of the 80-kVp DECT spectrum. Therefore, their CT numbers in the 80-kVp data are subtly affected by the small changes with varying phantom diameter in the mean energies of transmitted (post-patient)

80-kVp spectra. These effects are modeled by differing constituent water and iodine density distributions in the 60-keV VMS images. Therefore, inconsistencies may arise at DECT VMS in materials which have their k-edge energy near the mean energy of either DECT spectrum, which the software is not explicitly modeling using the current choice of basis materials. However, this limitation can be overcome for future dual-contrast-agent DECT technology by developing multi-material DECT material decomposition algorithms that include the k-edge effects of injected agents. Overall, however, the 60- and 80-keV VMS levels, suggested by Gabbai *et al.*,(8) are good surrogates for the mean energies of the transmitted 80-kVp and 140-kVp spectra, and could substitute for separate SECT acquisitions for this type of research.

Our study had several limitations. First, only one dual-energy platform, rapid-kVp-switching DECT, was used. Results may vary slightly with different types of DECT scanners; however, prior comparisons of DERs yielded similar results between scanner types,(8) and a previous study using DSCT showed a size-independent DER for iodine.(13) Furthermore, in our study, the DECT and SECT results were similar, which further suggests that the consistency of the DERs is platform independent. Similarly, we did not explore the alternative tube potentials available on recent DSCT scanners (70 and 100 kVp for the low-energy acquisition and 150 kVp for the high-energy acquisition). Although the DERs themselves would likely change when using different tube potentials,(7) we anticipate that the DERs resulting from a given choice of tube potentials would remain independent of phantom size. Second, only phantoms were used. Complex patient anatomy and its interaction with contrast material were not investigated. Again, this is unlikely to affect the underlying physical attenuation processes, and our result of consistent DERs over various phantom sizes is likely to hold true in a clinical setting. Third, only a selection of contrast-producing elements was investigated. Omissions which have been proposed as possible high-Z contrast materials include gold and ytterbium.(25, 26) However, these elements have atomic numbers within the range investigated in this study, and as such, are likely to produce similar results. Finally, we tested only single concentrations of each element. Nevertheless, prior studies showed that the DER is independent of elemental concentration.(4, 8)

To conclude, we found that dual-energy ratios are independent of phantom size for a range of contrast-producing elements. This result is encouraging for future material-discrimination efforts, and for the development of new high-Z contrast media for dual-contrast-agent CT scanning techniques. High-Z materials should be robustly separable from biological tissues and conventional contrast agents across the wide range of patient sizes encountered clinically.

Acknowledgments

Funding information: Research reported in this publication was supported by the National Institute of Biomedical Imaging and Bioengineering of the National Institutes of Health under Award Number R01EB015476. The content is solely the responsibility of the authors and does not necessarily represent the official views of the National Institutes of Health.

References

1. Marin D, Boll DT, Mileto A, Nelson RC. State of the art: dual-energy CT of the abdomen. Radiology. 2014; 271(2):327–342. [PubMed: 24761954]
2. Johnson TR, Krauss B, Sedlmair M, et al. Material differentiation by dual energy CT: initial experience. Eur Radiol. 2007; 17(6):1510–1517. [PubMed: 17151859]
3. Zhang LJ, Peng J, Wu SY, et al. Liver virtual non-enhanced CT with dual-source, dual-energy CT: a preliminary study. Eur Radiol. 2010; 20(9):2257–2264. [PubMed: 20393717]
4. Tran DN, Straka M, Roos JE, Napel S, Fleischmann D. Dual-energy CT discrimination of iodine and calcium: experimental results and implications for lower extremity CT angiography. Acad Radiol. 2009; 16(2):160–171. [PubMed: 19124101]
5. Wang J, Garg N, Duan X, et al. Quantification of iron in the presence of calcium with dual-energy computed tomography (DECT) in an ex vivo porcine plaque model. Phys Med Biol. 2011; 56(22): 7305. [PubMed: 22036792]
6. Fischer MA, Reiner CS, Raptis D, et al. Quantification of liver iron content with CT—added value of dual-energy. Eur Radiol. 2011; 21(8):1727–1732. [PubMed: 21472472]
7. Falt T, Soderberg M, Wasselius J, Leander P. Material Decomposition in Dual-Energy Computed Tomography Separates High-Z Elements From Iodine, Identifying Potential Contrast Media Tailored for Dual Contrast Medium Examinations. J Comput Assist Tomogr. 2015
8. Gabbai M, Leichter I, Mahgerefteh S, Sosna J. Spectral material characterization with dual-energy CT: comparison of commercial and investigative technologies in phantoms. Acta Radiol. 2015; 56(8):960–969. [PubMed: 25182803]
9. Nowak T, Hupfer M, Brauweiler R, Eisa F, Kalender WA. Potential of high-Z contrast agents in clinical contrast-enhanced computed tomography. Med Phys. 2011; 38(12):6469–6482. [PubMed: 22149830]
10. FitzGerald PF, Colborn RE, Edic PM, et al. CT Image Contrast of High-Z Elements: Phantom Imaging Studies and Clinical Implications. Radiology. 2016; 278(3):723–733. [PubMed: 26356064]
11. Brooks RA, Di Chiro G. Beam hardening in x-ray reconstructive tomography. Phys Med Biol. 1976; 21(3):390–398. [PubMed: 778862]
12. Schindera ST, Tock I, Marin D, et al. Effect of beam hardening on arterial enhancement in thoracoabdominal CT angiography with increasing patient size: an in vitro and in vivo study. Radiology. 2010; 256(2):528–535. [PubMed: 20656839]
13. Krauss B, Grant KL, Schmidt BT, Flohr TG. The importance of spectral separation: an assessment of dual-energy spectral separation for quantitative ability and dose efficiency. Invest Radiol. 2015; 50(2):114–118. [PubMed: 25373305]
14. Boone, JM., Strauss, KJ., Cody, DD., et al. Report of AAPM Task Group 204 College. Park, MD: American Association of Physicists in Medicine; 2011. Size-Specific Dose Estimates (SSDE) in Pediatric and Adult Body CT Examinations.
15. Frenzel T, Lawaczeck R, Taupitz M, et al. Contrast Media for X-ray and Magnetic Resonance Imaging: Development, Current Status and Future Perspectives. Invest Radiol. 2015; 50(9):671–678. [PubMed: 26207928]
16. Torres AS, Bonitatibus PJ Jr, Colborn RE, et al. Biological performance of a size-fractionated core-shell tantalum oxide nanoparticle x-ray contrast agent. Invest Radiol. 2012; 47(10):578–587. [PubMed: 22836312]
17. Mongan J, Rathnayake S, Fu Y, et al. In vivo differentiation of complementary contrast media at dual-energy CT. Radiology. 2012; 265(1):267–272. [PubMed: 22778447]
18. Roessler AC, Hupfer M, Kolditz D, Jost G, Pietsch H, Kalender WA. High Atomic Number Contrast Media Offer Potential for Radiation Dose Reduction in Contrast-Enhanced Computed Tomography. Invest Radiol. 2016; 51(4):249–254. [PubMed: 26606552]
19. Jakhmola A, Anton N, Anton H, et al. Poly-epsilon-caprolactone tungsten oxide nanoparticles as a contrast agent for X-ray computed tomography. Biomaterials. 2014; 35(9):2981–2986. [PubMed: 24393266]

20. Lambert JW, Edic P, Fitzgerald PF, Torres AS, Yeh BM. Complementary contrast media for metal artifact reduction in Dual-Energy CT. J Med Imaging. 2015; 2(3):033503.

21. Lee N, Choi SH, Hyeon T. Nano - Sized CT Contrast Agents. Advanced Materials. 2013; 25(19): 2641–2660. [PubMed: 23553799]

22. Silvestri A, Polito L, Bellani G, et al. Gold nanoparticles obtained by aqueous digestive ripening: Their application as X-ray contrast agents. J Colloid Interface Sci. 2015; 439:28–33. [PubMed: 25463172]

23. FitzGerald PF, Butts MD, Roberts JC, et al. A Proposed Computed Tomography Contrast Agent Using Carboxybetaine Zwitterionic Tantalum Oxide Nanoparticles: Imaging, Biological, and Physicochemical Performance. Invest Radiol. 2016

24. Yu L, Leng S, McCollough CH. Dual-Energy CT–Based Monochromatic Imaging. Am J Roentgenol. 2012; 199(5_supplement):S9–S15. [PubMed: 23097173]

25. Hainfeld J, Slatkin D, Focella T, Smilowitz H. Gold nanoparticles: a new X-ray contrast agent. Br J Radiol. 2014; 79(939):248–253.

26. Liu Y, Ai K, Liu J, Yuan Q, He Y, Lu L. A High - Performance Ytterbium - Based Nanoparticulate Contrast Agent for In Vivo X - Ray Computed Tomography Imaging. Angew Chem Int Ed Engl. 2012; 51(6):1437–1442. [PubMed: 22223303]

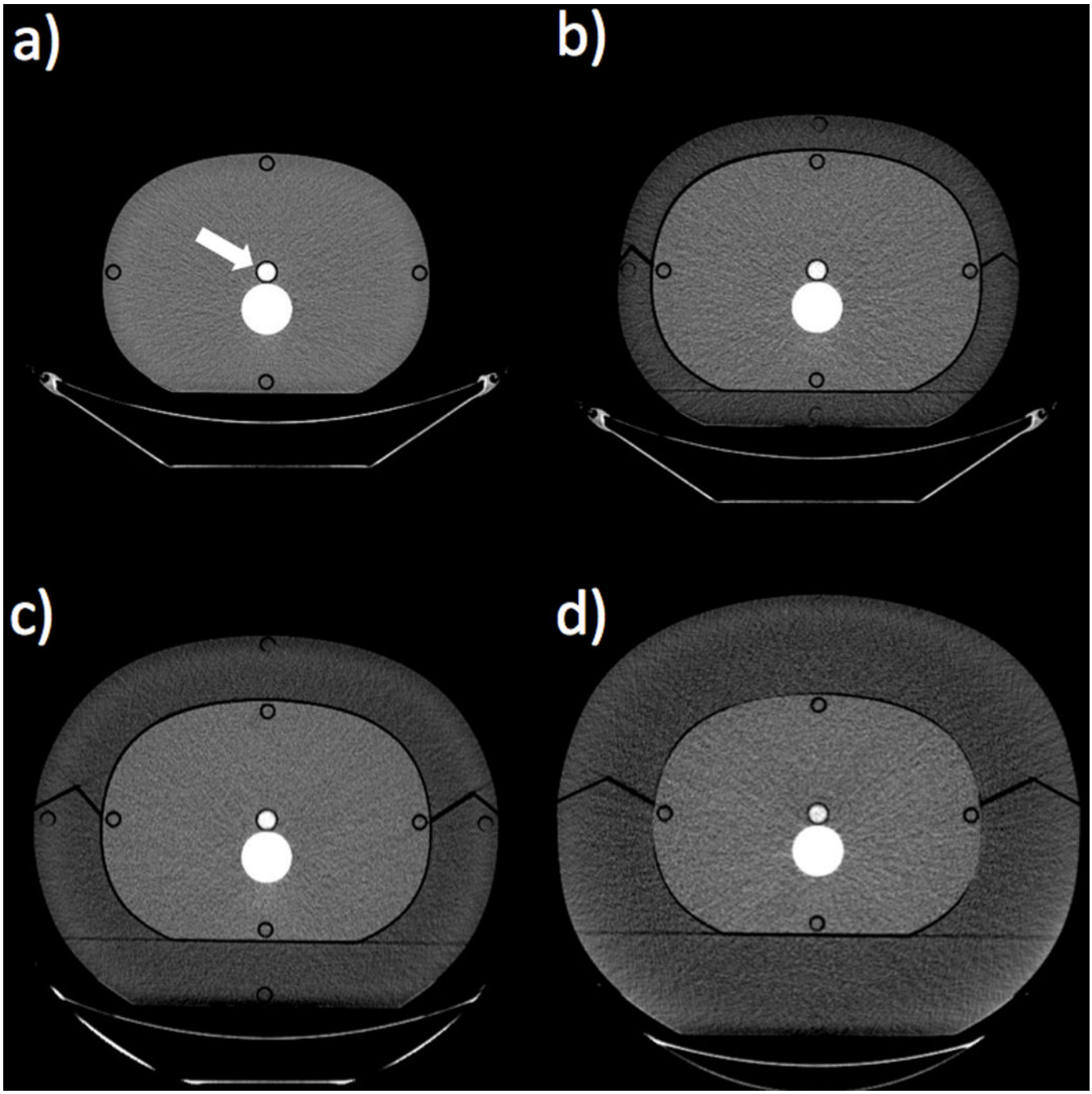

Figure 1.

Axial CT images showing the four phantom size configurations. The white arrow shows the location of the contrast vial, immediately anterior to the spine insert (Window Width = 400; Window Level = 40). a) Base phantom composed of soft-tissue-equivalent plastic, outer diameter = 220 × 300 mm. b) Base phantom with a 33-mm-thick fat ring composed of adipose-equivalent plastic, outer diameter = 285 × 365 mm. c) Base phantom with a 60-mm-thick fat ring, outer diameter = 340 × 420 mm. d) Base phantom with a 90-mm-thick fat ring, outer diameter = 400 × 480 mm.

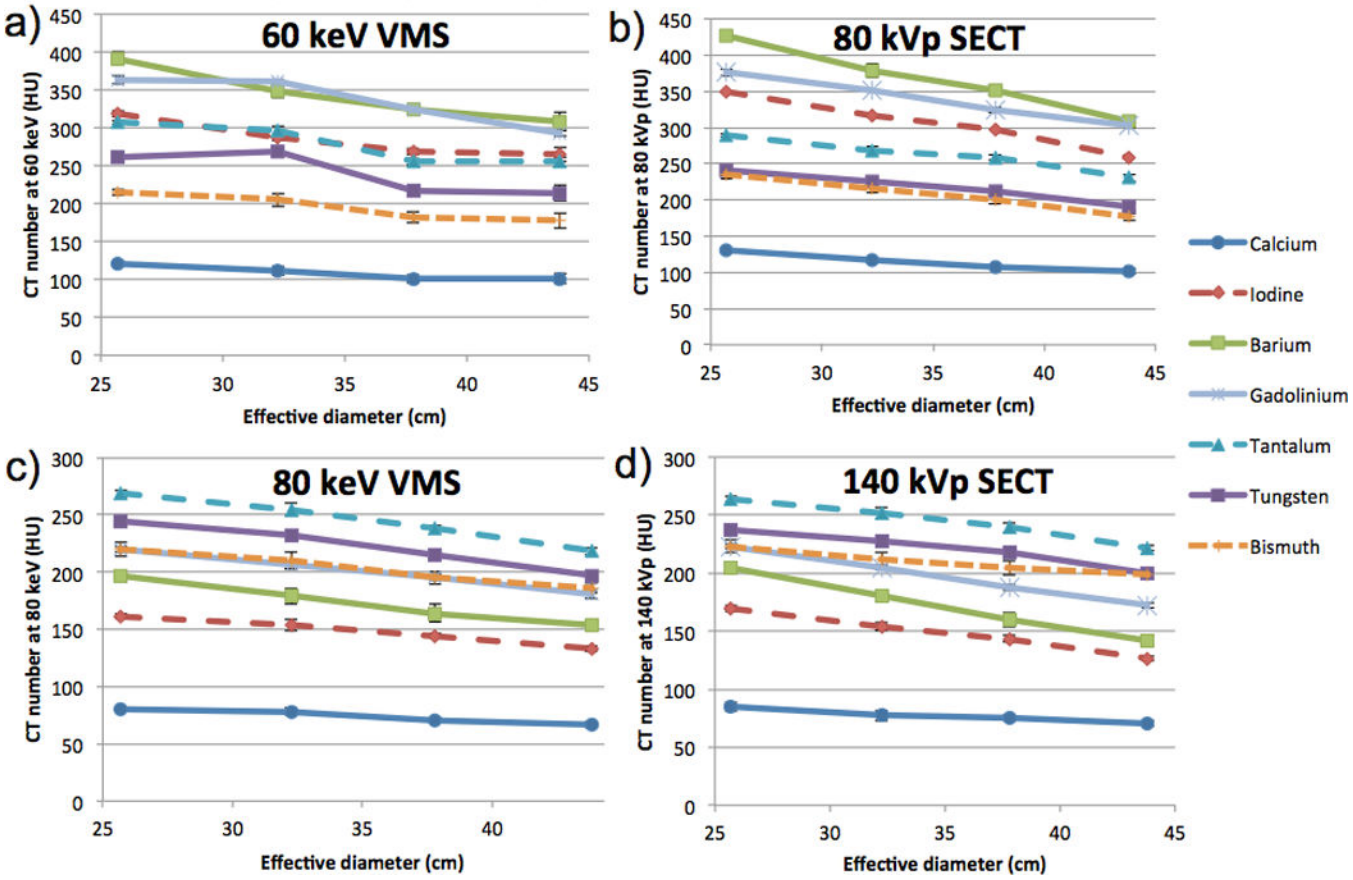

Figure 2.

CT number versus effective phantom diameter for the seven contrast elements. a) CT number at 60-keV VMS from DECT. b) CT number at 80-kVp from SECT. c) CT number at 80-keV VMS from DECT. d) CT number at 140-kVp from SECT. Error bars represent the +/− the standard deviation among the 10 measurements taken for each data point, and are generally too small to see in these plots.

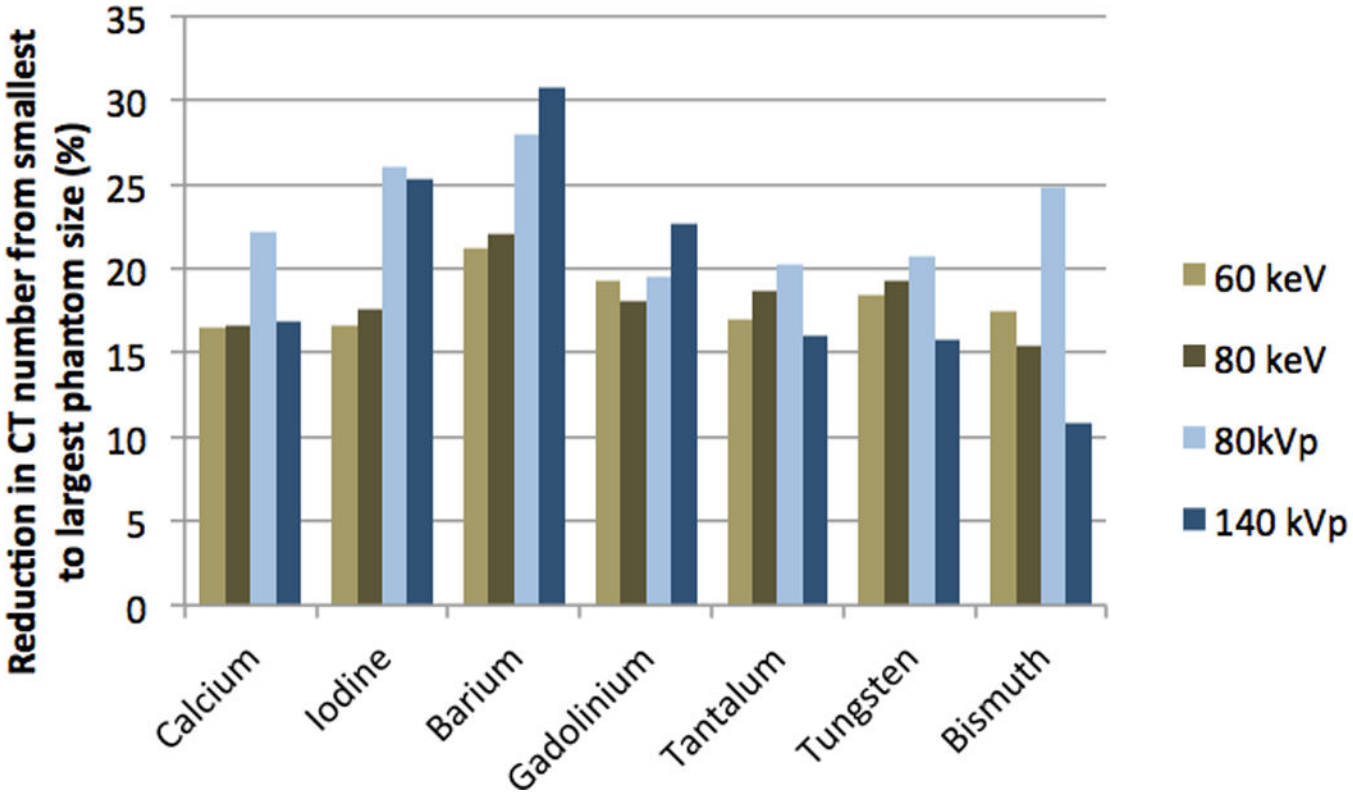

Figure 3.
Percentage reduction in CT number from smallest (257 mm effective diameter) to the largest (438 mm effective diameter) phantom size.

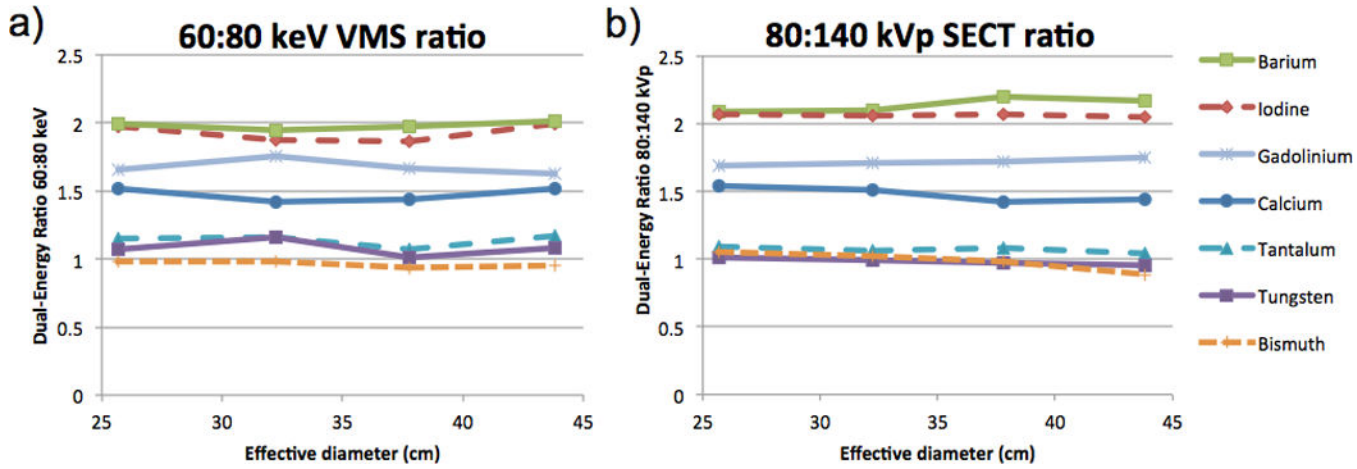

Figure 4.

Dual-energy ratio versus phantom effective diameter for the seven contrast elements. a) 60:80-keV VMS dual-energy ratio. b) 80:140-kVp SECT dual-energy ratio.

Table 1

Phantom configurations and scan details. The effective diameter is defined as $\sqrt{AP \times LAT}$ where AP and LAT are the anterior-posterior and lateral diameters, respectively. The tube current-time product is defined as the product of the instantaneous tube current (mA) and the gantry rotation time (s).

Phantom Configuration	Fat ring thickness (mm)	Outer AP diameter (mm)	Outer LAT diameter (mm)	Effective Diameter (mm)	SECT tube current-time product (mAs)		SECT CTDIvol (mGy)		GSI protocol number	DECT tube current-time product (mAs)	*DECT CTDIvol (mGy)
					80 kVp	140 kVp	80 kVp	140 kVp			
1	—	220	300	257	214	45	6.36	6.36	48	182	8.9
2	33	285	365	323	350	85	10.4	10.7	44	193	10.5
3	60	340	420	378	920	215	24.9	24.6	10	480	25.1
4	90	400	480	438	1400	600	37.9	68.6	5	600	32.0

*The smaller range in DECT CTDIvol compared to the SECT CTDIvol reflects the available GSI protocol options.

Table 2

Specification of the contrast elements

Element	Atomic number	K edge energy (keV)	Compound used	Chemical formula	Solvent/ suspension	Concentration (mg active element/mL)
Calcium	20	4.0	Calcium carbonate	$CaCO_3$	water with % xanthan gum	30
Iodine	53	33.2	Iohexol	$C_{19}H_{26}I_3N_3O_9$	water	10
Barium	56	37.4	Barium sulphate	$BaSO_4$	water with 1% xanthan gum	10
Gadolinium	64	50.2	Gadobenate dimeglumine	$C_{22}H_{28}GdN_3O_{11} \cdot 2C_7H_{17}NO_5$	water	10
Tantalum	73	67.4	Tantalum oxide nanoparticles	$(Ta_2O_5)(C_7H_{14}NO_5Si)_{2.8}$	water	10
Tungsten	74	69.5	Sodium tungsten dihydrate	$Na_2WO_4 \cdot 2H_2O$	water	10
Bismuth	83	90.5	Bismuth citrate	$C_6H_5BiO_7$	water with 1% xanthan gum	10

Table 3

Dual-energy ratio (DER) range for each element at dual-energy virtual monochromatic spectral (60:80 keV), and single-energy CT (80:140 kVp)

Element	DECT VMS 60:80-keV DER range	SECT 80:140-kVp DER range
Calcium	1.42 — 1.52	1.42 — 1.54
Iodine	1.86 — 1.99	2.04 — 2.07
Barium	1.95 — 2.01	2.09 — 2.20
Gadolinium	1.63 — 1.75	1.69 — 1.75
Tantalum	1.07 — 1.17	1.04 — 1.10
Tungsten	1.01 — 1.16	0.95 — 1.02
Bismuth	0.94 — 0.98	0.89 — 1.05

Table 4

Percentage difference of the dual-energy ratio (DER) generated at dual-energy virtual monochromatic spectral (60:80 keV) and single-energy CT (80:140 kVp), for each element and phantom size. A positive value indicates a higher DER at DECT VMS.

	Percentage difference between VMS and SECT DERs at a phantom effective diameter of:			
Element	**257 mm**	**323 mm**	**378 mm**	**438 mm**
Calcium	−1.3	−6.2	0.8	5.5
Iodine	−4.7	−9.3	−10.2	−2.6
Barium	−4.8	−7.5	−10.2	−7.5
Gadolinium	−2.1	2.4	−3.6	−7.3
Tantalum	4.5	9.3	−1.3	12.4
Tungsten	5.6	16.6	3.7	13.6
Bismuth	−7.3	−4.6	−4.7	7.6